Microporous and Mesoporous Materials 170 (2013) 9–19

Contents lists available at SciVerse ScienceDirect

Microporous and Mesoporous Materials

journal homepage: www.elsevier.com/locate/micromeso

Surface silylation of mesoporous/macroporous diatomite (diatomaceous earth) and its function in Cu(II) adsorption: The effects of heating pretreatment

Peng Yuan [a,*], Dong Liu [a], Dao-Yong Tan [a,c], Kang-Kang Liu [b], Hua-Guang Yu [d], Yuan-Hong Zhong [a,c], Ai-Hua Yuan [b], Wen-Bin Yu [a,c], Hong-Ping He [a]

[a] CAS Key Laboratory of Mineralogy and Metallogeny, Guangzhou Institute of Geochemistry, Chinese Academy of Sciences, Wushan, Guangzhou 510640, China
[b] School of Material Science and Engineering, Jiangsu University of Science and Technology, Zhenjiang 212003, China
[c] Graduate School of the Chinese Academy of Science, Beijing 100049, China
[d] College of Physics Science and Technology, Yangzhou University, Yangzhou 225002, China

ARTICLE INFO

Article history:
Received 4 April 2012
Received in revised form 14 November 2012
Accepted 20 November 2012
Available online 2 December 2012

Keywords:
Diatomite
Heating
Silylation
Porosity
Cu(II)

ABSTRACT

The calcined product of naturally occurring porous diatomite was previously assumed to be structure-destroyed or at least surface-reconstructed and therefore unsuitable for surface silylation. The present study indicates that the porosity of the mesoporous/macroporous diatomite remains intact after calcination at temperatures as high as 800 °C, and the surface silylation of diatomite is achievable even for diatomite calcined at high temperatures. The interface interactions between the hydroxyl species of diatomite and γ-aminopropyltriethoxysilane (APTES) are significantly affected by heating pretreatment. Physically adsorbed water was largely preserved in diatomite at a low heating temperature, leading to the strong hydrolysis of APTES and the subsequent oligomerization between the hydrolyzed APTES species. Under heating at high temperature (800 °C), the isolated silanols initially covered by water molecules were exposed and available for the direct grafting of APTES, forming a grafting-dominant structure with high thermal stability (540 °C). The grafting-dominant diatomite had a much higher Cu(II) adsorption than the oligomerization-dominant type, because the coordination between the copper and nitrogen was stronger in the former case. These results demonstrate that heating pretreatment plays a key role in the surface silylation of diatomite, and that Cu(II) adsorption is highly dependent on the surface structure of the silylated diatomite.

1. Introduction

Diatomite, also known as diatomaceous earth or kieselgur, is a fossil assemblage of siliceous diatom frustules. Diatom frustules are mainly composed of amorphous hydrated silica ($SiO_2 \cdot nH_2O$), which is categorized as non-crystalline opal-A according to the mineralogical classification [1,2]. Diatomite is easily available at a low cost because diatomaceous silica is the most abundant form of silica on earth. Diatomite also has many unique physical and chemical characteristics [3–6], such as highly developed mesoporosity and/or macroporosity, strong acid resistance, high mechanical strength and low thermal conductivity, enabling their wide uses in a variety of applications for high-performance technologies (e.g., microelectronics, chemo- and bio-sensors, and transducers) or as fillers, filters or supports, catalysts, adsorbents, and mild abrasives [4,7,8]. In particular, diatomite has been predominantly used as a filtration medium (e.g., filter aid) [9] for purifying various beverages and for gasification applications in fluidized bed reactors [4]. A key reason for the use of diatomite as a filtration medium is that the bimodal mesoporosity/macroporosity of diatom frustules is usually desirable for filtration because mesopores enhance the specific surface area, while macropores increase the efficiency of the mass-transport and diffusion processes. Another reason is that the diatom frustules are rigid and naturally separated. Depending on the diatom species, the dimensions of frustules range from <1 to >100 μm (usually more than 10 μm) [4]. Therefore, the voids between the frustules are capacious and strong enough to maintain a high filtering velocity and to avoid the blocking of the filtering cake [1,8,9]. As a result, a diatomite-based filtering system is significantly more efficient in removing tiny solid particles in different liquids than other natural materials (such as zeolite and clay minerals) [8,9].

In addition, naturally occurring diatomite with a mesoporous/macroporous structure possesses good adsorptive properties and has been used for the adsorption of metal ions or organic molecules in aqueous solution. The adsorptions of some metal ions (e.g., Ni(II) [10,11], Pb(II) [11–13], Cu(II) [11], Cd(II) [13] and Th(IV) [14]) and organic contaminants [15] on raw diatomite and the effects of aqueous chemistry conditions, such as pH and

* Corresponding author. Tel./fax: +86 20 85290341.
E-mail address: yuanpeng@gig.ac.cn (P. Yuan).

1387-1811/$ - see front matter © 2012 Elsevier Inc. All rights reserved.
http://dx.doi.org/10.1016/j.micromeso.2012.11.030

temperature, on the adsorptions have been comprehensively investigated. However, diatomite exhibited an ordinary adsorption capacity for these molecules or ions that was close to or even lower than those of natural zeolite [16] or clay minerals, such as kaolinite [17] and montmorillonite [17,18]. This difference in adsorption capacity is due to the fact that the aforementioned adsorbates are too small to be filtered by the micron- or nanometer-sized channel of diatomite, and the surface silanols (i.e., Si–OH) of diatom frustules do not possess a strong adsorption affinity for these adsorbates; moreover, the ionic exchange capacity of diatomite is much smaller than that of zeolite or montmorillonite [16,18]. It is noteworthy that the adsorption capacity of some metal ions on diatomite is likely to be overestimated in the literature, because considerable clay mineral impurities were shown in the diatomite samples utilized [13,14], as evidenced by the high Al_2O_3 content (10–20 wt.%), and many clay minerals possess much higher metal adsorption capacities than natural silica [17,18]. However, this overestimation on the adsorption capacity of diatomite has not yet received sufficient attention.

Increasing attention has been paid to modifying the surface of diatomite by using surfactants or inorganic coatings to improve its adsorption of some organic or bioactive target molecules (e.g., dyes and viruses) to make diatomite versatile for both filtering and adsorption [19–24]. In contrast, much less efforts have been made to enhance the adsorption of heavy-metal ions on diatomite [25,26], even though the heavy-metal adsorption is associated with extensive demands for the remediation of heavy-metal pollution, noble metal recovery, and metal supporting for catalysis purposes. Surface silylation by using organosilane with metal-affinitive groups has been applied to several types of synthetic silicas to improve their heavy-metal adsorption, particularly in the cases of ordered mesoporous silica, such as MCM41 and SBA15 [27,28]. However, these silica materials are too expensive to produce to enable their large-scale utilization in the field of adsorption or filtering. In this sense, the organosilane modification of naturally occurring mesoporous/macroporous diatomite for metal adsorption purposes is of great significance. Through surface silylation, the metal chelating functionality (such as by an amino or mercapto group) can be introduced to overcome the inherent limitations (e.g., low adsorption capacity, weak binding strength and low selectivity) of diatomite for metal adsorption.

Unfortunately, the organosilane modification of mesoporous/macroporous diatomite has so far been rarely investigated [29]. This is most likely because the commercial diatomite used for filtering is actually the calcined product that already underwent calcination at 600–1100 °C [7,9], and is thus supposed to be structure-destroyed or at least surface-reconstructed and therefore unsuitable for surface silylation. This scenario is quite unlike the case of ordered mesoporous materials, which do not undergo any thermal treatment before silylation [28]. In a very recent report, Losic et al. demonstrated the effects of 3-mercaptopropyltrimethoxysilane modification on improving the Au(III) adsorption of diatom silica [30]; however, litter attention was paid to the roles of the hydroxyl species at the surfaces of diatom silica in the silylation process.

It is noteworthy that our previous study indicated that the surface reconstruction of diatomaceous silica, i.e., the complete dehydroxylation of silanols and the formation of siloxane, occurs at a higher temperature (approximately 1000–1100 °C) than generally postulated [31,32]. This result implies that a considerable number of silanols may exist after calcination and possibly be available for organosilane grafting. However, the problems of whether or how the evolution of different hydration states during the dehydration and dehydroxylation processes affects the surface silylation of diatomite and how the porosity of diatomite changes after calcination and silylation still remain unknown; therefore, these problems very deserve further investigation.

In the present work, various chemical, textural (nitrogen adsorption–desorption isotherms), spectroscopic (Fourier-transform infrared spectroscopy, thermogravimetry and X-ray photoelectron spectroscopy) and microscopic (scanning electron microscopy and transmission electron microscopy) characterization techniques were used to study the key mechanism of how the evolution of the porosity and hydration states of diatomite under heating influences the organosilane functionalization process. γ-Aminopropyltriethoxysilane (APTES, $H_2NCH_2CH_2CH_2Si_4(OCH_2CH_3)_3$) was used to the silylate the diatomite. The raw diatomite sample was carefully purified to reduce the influences of the impurities. Cu(II) was selected as a model guest ion and used for the uptake tests to explore how the silylation corresponding to different heating pretreatments affects the heavy metal binding properties of the functionalized diatomite adsorbents. The fundamental information derived from this study is important for the versatile uses of diatomite in any fields related to metal ion adsorption.

2. Experimental methods

2.1. Materials and methods

A raw diatomite sample was obtained from Changbai deposit in Jiling Province, China. Purifying the raw diatomite involved the commonly used sedimentation method followed by an acid-washing process, in which a 2 M HCl solution was used and the mixture was kept at 105 °C for 4 h, with a ratio of HCl solution:diatomite of 15 cm^3:1 g of diatomite. At the end of the acid-washing process, the diatomite dispersion was centrifuged and washed repeatedly until it was free of Cl^- (tested by $AgNO_3$). The purified diatomite was dried at 150 °C for 24 h and ground into powder in a mortar. The product was denoted Dt. The chemical composition (wt.%) of Dt was as follows: SiO_2, 94.74; Al_2O_3, 2.11; Fe_2O_3, 0.23; K_2O, 0.43; CaO, 0.15; TiO_2, 0.14; and ignition loss, 2.72. The heat pretreatment of Dt was performed in a programmed temperature-controlled muffle oven at 400, 600, 800, 1000 and 1100 °C for 1 h, and the obtained samples were denoted Dt-400, Dt-600, Dt-800, Dt-1000 and Dt-1100, respectively.

Organosilane-modified diatomite samples were prepared according to the following procedures: 4 mL of APTES was dissolved in 50 mL of dry toluene (AR grade), and approximately 1 g of diatomite powder was added to the APTES/toluene mixture. The mixture was then ultrasonically dispersed for 0.5 h. After that, the suspension was refluxed at 120 °C for 20 h under constant stirring (400 rpm). In the refluxing system, a calcium chloride drying tube was attached to the end and the reaction system was placed under an N_2 atmosphere to ensure a dry environment. The solid phase in the resultant mixture was filtered, extensively washed six times with fresh toluene to remove the excess organosilane, and then dried overnight at 90 °C for further curing. The APTES (99%, Aldrich) was used as received. Toluene was used after distillation over activated molecular sieves. The APTES-modified diatomite samples are differentiated by the suffix "/M"; for example, Dt-400/M denotes the diatomite-based material that was thermally treated at 400 °C and further modified by using ATPES.

In a typical run of the Cu(II) adsorption test, 0.1 g of diatomite adsorbent was added to a Cu(II) solution with the scheduled concentration in a 100-mL polyethylene bottle. The Cu(II) solution was prepared by dissolving $CuSO_4{\cdot}5H_2O$ in distilled water. To test the adsorption kinetics, the mixture in the polyethylene bottle was strongly shaken at a rate of 150 rpm in an oscillator to ensure complete mixing. The contact time ranged from 5 to 720 min. At timed intervals, the mixture was centrifuged and the supernatant was used to determine the Cu(II) content by a PE-3100 atomic absorption spectroscopy. The experiments performed to obtain

the adsorption isotherms followed a very similar procedure, except the equilibrium time was fixed at 480 min. The adsorption results were corrected by performing blank tests in which no adsorbent was added to the Cu(II) solution. The amount of Cu(II) adsorbed per unit mass of the adsorbent, q (mg/g), was computed by using the expression $q = (C_0 - C_t)/m$, where C_0 and C_t (mg/L) are the concentrations of Cu(II) in the reaction solution before and after treatment, respectively, and m (g) is the amount of adsorbent in 1 L of Cu(II) solution. The removal efficiency of Cu(II), E (%), was calculated using the equation $E = [(C_0 - C_t)/C_0] \times 100$.

2.2. Characterization methods

The X-ray diffraction (XRD) patterns were obtained with a Bruker D8 Advance diffractometer with an Ni filter and CuKa radiation ($\lambda = 0.154$ nm) using a generator voltage of 40 kV, a current of 40 mA, and a scan rate of 1° (2θ)/min. N_2 adsorption–desorption isotherms were measured on a Micromeritics ASAP2020 system at liquid-nitrogen temperature. Samples were outgassed at 110 °C for 8 h before measurement. The specific surface area, S_{BET}, was calculated using the multiple-point Brunauer-Emmett-Teller (BET) method, and the total pore volume, V_{pore}, was evaluated based on nitrogen uptake at a relative pressure of approximately 0.99.

The CHN elemental analysis was performed with a Vario El III elemental analyzer. The contents of the loaded APTES (mmol/g) in the modified diatomite samples were calculated from the content (wt.%) of N obtained by CHN analysis in which the content of N in original diatomite had been subtracted.

The thermogravimetric (TG) analysis was conducted on a Netzsch STA 409PC instrument. Approximately 10 mg of the sample was heated in a corundum crucible. The sample was heated from 30 to 1000 °C at a heating rate of 5 °C/min under a highly pure N_2 atmosphere (20 cm^3/min).

The solid-state NMR experiments were carried out at $B_0 = 9.4$ T on a Bruker AVANCE III 400 WB spectrometer. The corresponding resonance frequency of ^{29}Si was 79.5 MHz. Samples were packed in a 7 mm ZrO_2 rotor and spun at the magic angle (54.7°), and the spinning rate was 7 kHz. ^{29}Si MAS NMR spectra were acquired using a 90° pulse of 6.0 μs and a recycle delay of 60 s. The ^{29}Si chemical shift was referenced to kaolinite at −91.5 ppm. For better resolved MAS NMR spectra, Gauss deconvolution by curve-fitting was applied to give the exact position, relative intensity, and area of each chemical shift signal. The fitting goodness (R^2) values for all NMR spectra are $\geqslant 0.996$.

Fourier-transform infrared spectroscopy (FTIR) spectra of the samples were recorded on a Bruker Vertex-70 Fourier-transform infrared spectrometer. The specimens were prepared for measurement by mixing 0.9 mg of the sample powder with 70 mg of KBr and pressing the mixture into a pellet. Over 64 scans were collected for each measurement at a resolution of 2 cm^{-1}.

Scanning electron microscopy (SEM) micrographs were obtained using a 5-kV FEI-Sirion 200 field emission scanning electron microscope. Transmission electron microscopy (TEM) images were obtained using a JEOL JEM-2100 electron microscope operating at an acceleration voltage of 200 kV. The specimens were prepared by the following procedure: the diatomite sample was ultrasonically dispersed in ethanol for 5 min, and a drop of the sample suspension was then dropped onto a carbon-coated copper grid, which was left to stand for 10 min before being transferred into the microscope.

X-ray photoelectron spectroscopy (XPS) data were obtained using an ultra-high vacuum XPS system (Kratos Amicus), equipped with monochromatic Mg K_α radiation (12 kV, 180 W). The pressure in the analysis chamber was maintained at 10^{-6} Torr or lower. All binding energies were referenced to the C1s hydrocarbon peak at 284.6 eV.

3. Results and discussion

3.1. The original diatomite and its structural and textural changes resulting from calcination

As showed by the SEM and bright-field TEM images (Fig. 1a and b), the dominant diatom of sample Dt, which is disc-shaped and has highly developed macroporous and mesoporous structure, is classified in the genus *Coscinodiscus* Ehrenberg (*Centrales*). The mesopore sizes, ranging from 20 to 50 nm, were determined from different TEM images. The diatom frustules are relatively uniform in diameter (20–40 μm) and thickness (1.2–1.8 μm). The XRD pattern of Dt (Fig. 1c) is characteristic of one broad peak centered at 21.8° (2θ) with a d spacing of 0.409 nm, which is in good agreement with that of the reference amorphous Opal-A. A small quantity of quartz impurity (<3 wt.%, based on a semi-quantitative calculation) is also contained in Dt (Fig. 1c). The specific surface area and pore volume of Dt are 25.2 m^2/g and 0.065 cm^3/g, respectively.

Two mass losses are resolved in the TG curve (Fig. 1d) of Dt. The mass loss in the temperature range of 30–200 °C, with a related DTG peak centered at 80 °C, is mainly ascribed to the dehydration of diatomite (Fig. 1d). This mass loss is very small because Dt was heated at 150 °C. The second mass loss is a gradual and slow loss, which occurs in the temperature range of 300–1000 °C and corresponds to the broad and poorly resolved DTG peak centered at approximately 600 °C. This mass loss is attributed to the dehydroxylation of the silanols of Dt.

Thermal treatment did not dramatically alter the diatomite mineral structure until 1200 °C, as indicated by the fact that the XRD patterns of diatomites heated at temperatures lower than 1200 °C remained unchanged. However, the XRD pattern of Dt-1200 is representative of the transformation of diatomaceous amorphous silica into the cristobalite phase (see Supplementary Fig. S1).

As shown in Fig. 2a, the nitrogen adsorption/desorption isotherm of Dt is characterized as a type II isotherm with an H3 hysteresis loop, according to the IUPAC classification [33]. The hysteresis is associated with the filling and emptying of the mesopores by capillary condensation. Calcination at temperatures lower than 800 °C did not evidently change the shape of the isotherms of the heated diatomite samples (Fig. 2a). However, calcination at higher temperatures resulted in a dramatic decrease in nitrogen adsorption and a weakening of the hysteresis, reflecting the deconstruction of the diatom frustule mesoporous structure.

The deconstruction of the porous diatom skeleton occurred at approximately 1100 °C, before the phase transition from the amorphous silica to cristobalite. The deconstruction is evidenced by the fact that the specific surface area and the pore volume of Dt-1100 are 4.9 m^2/g and 0.017 cm^3/g, respectively, which are significantly smaller than those of Dt (Fig. 2b). The diatom frustule decomposition may begin in the range of 800–1000 °C because Dt-1000 exhibits an evident decrease in the specific surface area and pore volume in this temperature range, whereas Dt-800 only shows a slight change in the specific surface area in the same temperature range (Fig. 2b). The textural parameters of the diatomite samples heated at different temperatures are summarized in Fig. 2b.

Fig. 3 displays the FTIR spectra of diatomite heated at different temperatures. The frequency and assignment of each vibration observed are listed in Table 1. The spectrum of Dt shows only one broad band centered at approximately 3430 cm^{-1} (Fig. 3a) in the hydroxyl region (3000–4000 cm^{-1}), which is attributed to the OH

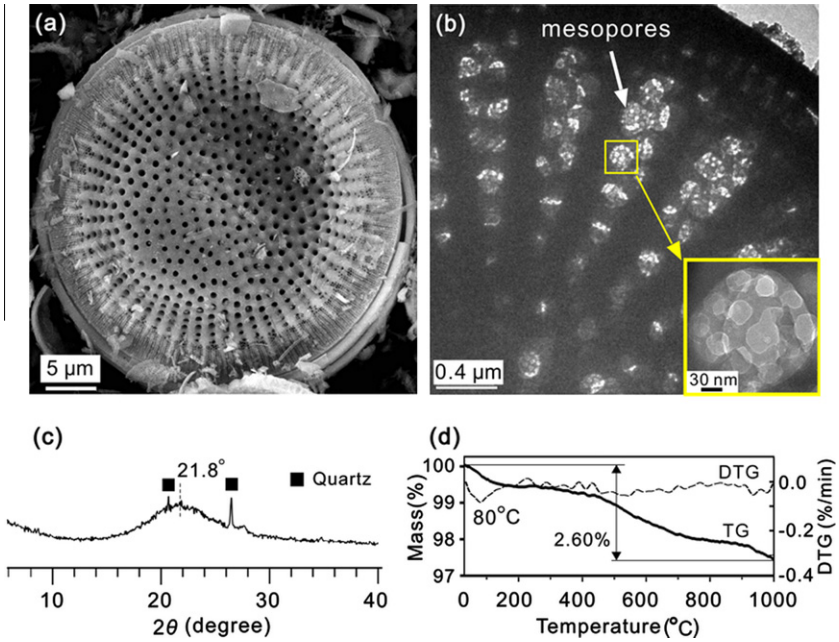

Fig. 1. (a) SEM and (b) bright-field TEM images of Dt; (c) XRD pattern of Dt; (d) TG/DTG curve of Dt.

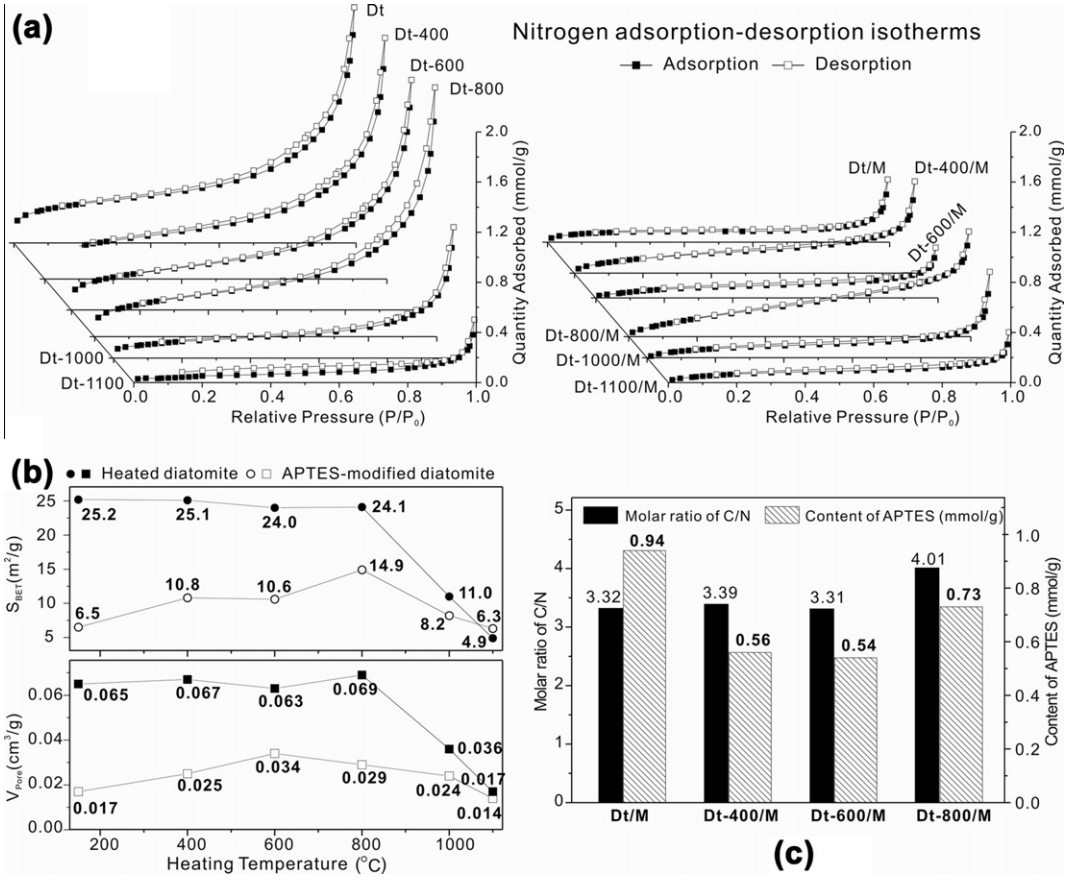

Fig. 2. (a) Nitrogen adsorption–desorption isotherms of diatomite samples; (b) The values of specific surface area and pore volume of the heated and APTES-modified diatomite samples; (c) the content of APTES in the modified diatomite samples.

vibration of the physically adsorbed H_2O. With increasing heating temperature, the intensity of the 3430 cm^{-1} band decreases and, finally, almost disappears at 1000 °C (Fig. 3a), corresponding to the gradual removal of the physically adsorbed water. Note that the diatomite sample is readily rehydrated, as is well known, so some water molecules may be re-adsorbed while preparing the sample and obtaining the spectrum.

A band at 3745 cm^{-1} is well resolved in the spectrum of Dt-800 (Fig. 3a). Its intensity evidently decreases in the spectrum of Dt-1000. This band is attributed to the isolated hydroxyl groups,

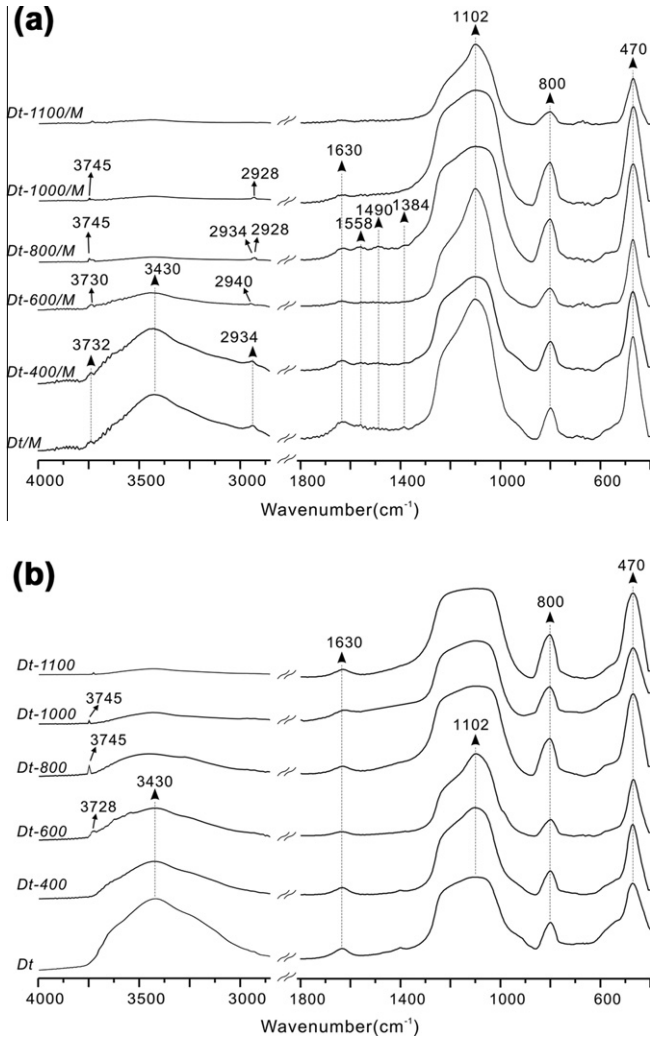

Fig. 3. FTIR spectra of (a) diatomite samples heated at different temperatures; and (b) APTES-modified diatomite samples.

which has been confirmed by various studies [32,39,40]. The band is not resolved in the spectra of diatomite samples heated at temperatures lower than 600 °C because the isolated hydroxyl groups are H-bonded with the physically adsorbed H_2O at these temperatures, such that their vibration signals are covered by the water signals. The evident weakening of the 3745 cm^{-1} band at 1000 °C indicates that most isolated silanols have been removed by condensation. This change is accompanied by the structure breakdown, as revealed by the dramatic decrease in porosity (Fig. 2b).

In addition, a poorly resolved band at approximately 3728 cm^{-1} is observed in the spectrum of Dt-600. It is attributed to the H-bonded silanols [39,41]. Silanols of this type are condensed more easily than the isolated silanols [32], so their vibration signals disappear in the spectrum of Dt-800.

Fig. 4a presents the ^{29}Si MAS NMR spectrum of Dt. The chemical shift signals at −111.7 ppm, −101.7 ppm, and −91.9 ppm are assigned to the siloxane bridge (Q^4 silicon, i.e., $Si(OSi)_4$), single silanols (Q^3, $Si(OSi)_3(OH)$), and geminal silanol (Q^2, $Si(OSi)_2(OH)_2$) of diatomaceous silica, respectively. The fractional population of silanol sites (F_s, %), is 20.6%, calculated from the equation $F_s = (A(Q^3) + A(Q^2))/(A(Q^4) + A(Q^3) + A(Q^2))$, where A is the peak area of the Q^i group [42]. The fractional population of germinal silanol sites (F_g, %) is only 6.4%, on the basis of the calculation using the equation $F_g = A(Q^2)/(A(Q^3) + A(Q^2))$. This result indicates that the single silanols are the primary population in the silanol groups of Dt. The ^{29}Si MAS NMR spectrum of Dt-800 (Fig. 4b) is analogous to that of Dt, where the F_s value of Dt-800 is slightly decreased to 17.5%, indicating that a small amount of silanols were condensed upon heating at 800 °C. It is noteworthy that the quantitative calculation of the silanols density, i.e., the number of OH groups per unit surface area, was not conducted on the basis of the obtained ^{29}Si MAS NMR results. The reason is that the presence of silicon circumstance of cyclic trisiloxane ring in the structure of diatomaceous silica has been demonstrated [43]; for this type of silica, ^{29}Si MAS NMR must be combined with Raman spectroscopy in evaluating the number of hydroxyls, otherwise the silanols density would be significantly overestimated. An in-depth explanation of this phenomenon and the related discussion has been given by Humbert [42].

3.2. Influences of heating on the surface organosilylation of diatomite

As shown in Fig. 2c, the modified diatomite samples exhibit evident APTES introduction, reflecting the success of the organosilane modification. The APTES content in the modified diatomites gradually decreases from the maximum (0.94 mmol/g for Dt/M) as the heating temperature increases, but Dt-800/M is an exception because its APTES content is higher than those of Dt-400/M and Dt-600/M (Fig. 2c).

The C/N molar ratios ($M_{C/N}$) of all modified diatomites are larger than the theoretical C/N molar ratio (3.0) of completely hydrolyzed APTES (Fig. 2c), indicating the incomplete hydrolysis of ethoxyl groups in APTES. This result implies that the physically adsorbed water molecules in diatomite are not sufficient to completely hydrolyze of APTES. Dt-800/M shows the lowest extent of APTES hydrolysis with the largest $M_{C/N}$ valueamong the APTES-modified samples (Fig. 2c), which is in agreement with the fact that the largest removal of the physically adsorbed water was demonstrated in Dt-800/M.

The FTIR spectra of the APTES-modified diatomites exhibit some new vibrations compared with those of the unmodified diatomites (Fig. 3b), including CH_2 stretching (2934 cm^{-1}), NH_2 deformation (1558 cm^{-1}), CH_2 deformation (1490 cm^{-1}), and CH_2 deformation (1384 cm^{-1}). These results confirm the success of the amine-modification.

The appearance of the aforementioned APTES vibrations is accompanied by the emergence of a 3732 cm^{-1} band in the spectrum of Dt/M (Fig. 3b). The 3732 cm^{-1} band is attributed to the O-H stretching of the silanols in the hydrolyzed APTES [44,45].

Table 1
Positions and assignments of the IR vibration bands [34–38].

Position (cm^{-1})	Assignments	Position (cm^{-1})	Assignments
3745	O–H stretching of isolated hydroxyl groups of diatomite	1558	N-H_2 deformation (scissoring)
3732, 3730	O–H stretching of hydrolyzed APTES	1490	C-H_2 deformation (scissoring)
3728	O–H stretching of H-bonded hydroxyl groups of diatomite	1384	C-H_2 deformation (wagging)
3430	O–H stretching of water	1102	In-plane Si–O stretching
2934, 2928	Symmetric C-H_2 stretching	800	Symmetric Si–O stretching
1630	O–H deformation of water	470	Si–O–Si deformation

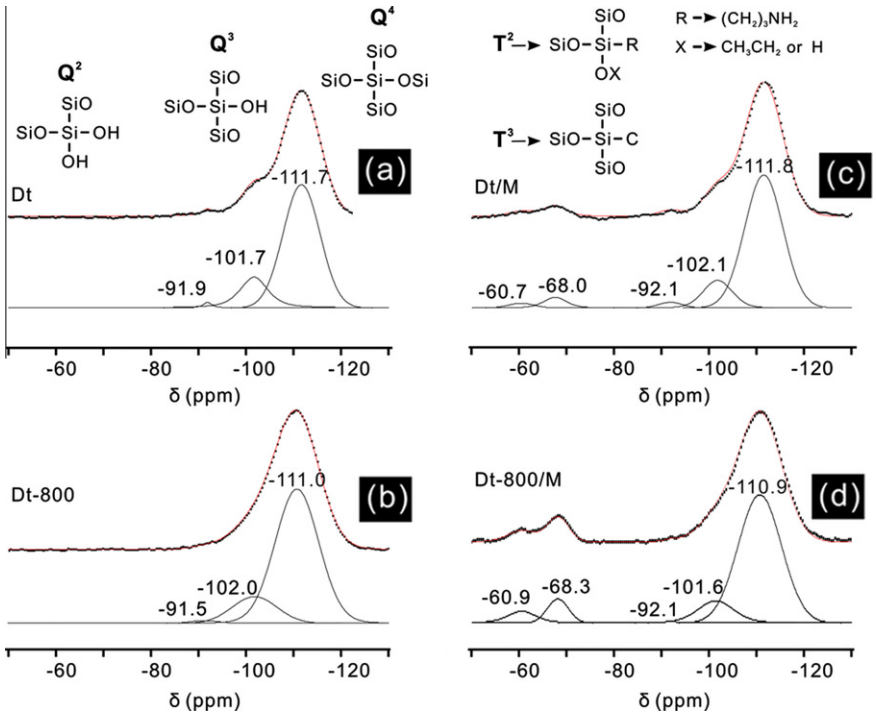

Fig. 4. ^{29}Si MAS NMR spectra of diatomite samples (dotted lines for experimental and solid lines for simulated).

The bands existence indicates that a large amount of silanols remain in Dt/M. Normally, the hydrolyzed APTES species are very readily condense with each other to form an oligomerized cross-linking framework [44], during which time the silanols of APTES should be consumed. Therefore, these remaining silanols may be sourced from the APTES molecules that were introduced into the framework through weak interactions, including hydrogen bonding, hydrophobic interactions, and Van der Waals interactions. Moreover, the chemical covalent grafting between the hydrolyzed APTES and the diatomite surface should be limited to a small scale because most surface silanols of diatomite in this case are covered by the H-bonded water molecules and above which, the physically adsorbed water molecules.

Quite different from the Dt/M case, the appearance of the APTES vibrations in the spectrum of Dt-800/M is accompanied by the dramatic weakening of the vibration (3745 cm^{-1}) of isolated silanol groups (Fig. 3b). This result reflects the occurrence of grafting between the hydrolyzed APTES and the surface silanols of diatomite. Some APTES molecules are very likely to be bonded to the diatomite silanols by direct condensation with a loss of ethanol [45,46] because the water molecules are not sufficient for APTES hydrolysis at 800 °C, as previously noted.

The APTES signals in the spectra of Dt-400/M and Dt-600/M (Fig. 3b) are weaker than those in the spectra of Dt/M and Dt-800/M, reflecting smaller contents of APTES. These results are in good agreement with the elemental analysis, which was expected due to the following reasons. The high APTES content in Dt/M is a result of the formation of the cross-linking framework of oligomerized APTES, which attracted and contained many APTES molecules through some weak interactions. In Dt-800/M, the APTES molecules were grafted onto the diatomite surface through strong chemical bonds scuh that the introduced APTES was not readily removed by washing in the preparation process. However, in the Dt-400/M or Dt-600/M case, the physically adsorbed water was largely removed, and the APTES molecules were not completely hydrolyzed to form oligomerized complexes. Moreover, the water molecules directly hydrogen-bonded with the silanols, so-called capping water molecules [31,47], still remained at 400 or 600 °C. As a result, the surface silanols were shielded from condensation with the APTES molecules by the capping water molecules. Accordingly, neither oligomerization among the APTES species nor grafting between APTES and diatomite occurred; therefore, the APTES species were dissociative in the hybrid and prone to removal by washing, leading to a low APTES content.

The N_2 adsorption–desorption isotherms of the APTES-modified diatomites (Fig. 2a) exhibit similar shapes to those of the unmodified diatomites, but with less developed hysteresis loops, which implies that the mesoporosity of the silylated diatomite is reduced. A decrease in the S_{BET} and V_{pore} values after APTES modification is also observed (Fig. 2b). The largest decrease in these values occurs in Dt/M, supporting the formation of the cross-linking framework composed of oligomerized APTES, which leads to the blocking of the diatomite pores. Dt-800/M exhibits a relatively small decrease in porosity and surface area, indicating that the APTES grafting layeron the diatomite surface is thin, thus causing the porosity to be mildly affected.

In the ^{29}Si MAS NMR spectrum of Dt/M (Fig. 4c), the chemical shifts at −68.0 ppm and −60.7 ppm are attributed to the tridentate (T^3) and bidentate (T^2) bonded silicons [46,48], respectively. The T^3 silicon represents that all the three ethoxyl groups of APTES were hydrolyzed and condensed with surface silanols of diatomite or with other hydrolyzed APTES; and T^2 means that some APTES species possess one ethoxyl (or hydroxyl) group that did not hydrolyze or condense (Fig. 4c). On the basis of the peak integration, the proportion of $T^3/(T^3 + T^2)$ for Dt/M is 70.5%, indicating that in this case the hydrolysis and condensation extent of APTES is high. The F_s value of Dt/M is 16.4%. This value is only slightly smaller than that of Dt, suggesting that the most silanols of diatomite did not involve into the condensation of APTES. That means the cross-linking frameworks were mainly composed of oligomerized APTES, which is consistent with the FTIR result. In contrast, the proportion of $T^3/(T^3 + T^2)$ for Dt-800/M (Fig. 4d) is 54.8%, which is substantially lower than that for Dt/M. This result indicates that much less hydrolysis and subsequent oligomerization of APTES occurred in Dt-800/M

than in Dt/M, owing to the removal of physical adsorbed water at 800 °C heating. This result implies that the APTES molecules were linked with diatomite through a direct condensation mechanism that was mentioned in the discussion on the FTIR results. It is noteworthy that quantitatively evaluating the different silicon environments is difficult, because some Q^4 and Q^3 silicons in the silylated diatomites were transformed from the initial Q^3 and Q^2 silicons owing to the grafting of APTES.

As shown in the TG/DTG curves of the APTES-modified diatomite samples, Dt/M exhibits two main mass losses, corresponding to the DTG peaks centered at 104 and 482 °C, respectively (Fig. 5a). The first mass loss in the range of 50–150 °C is attributed to the physically adsorbed APTES or the residual water. The second mass loss in the range of 150–800 °C is associated with a very broad DTG peak, implying that this loss was caused by several stages of thermal decomposition. These stages may include the removal of weakly bonded APTES species in the cross-linking framework, the decomposition of the oligomerized APTES, and the decomposition of the grafted APTES species, although the latter one should be very minor. Among these stages, the first two should occur at relatively low temperatures because the related weak interactions are less thermally stable than chemical covalent bonding, as is well known [42]. However, further specifying the exact boundaries of the removal of weakly bonded APTES species and the decomposition of the oligomerized species is difficult, because the related two procedures should partially overlap.

The mass loss of the physically adsorbed APTES in Dt-800/M is much smaller than that in Dt/M (Fig. 5d). In particular, a distinct DTG peak at 540 °C is resolved (Fig. 5d). This peak reflects a high thermally-stable state of APTES bonding, so it is attributed to the decomposition of the covalently bonded APTES. Such a high thermal-resistant performance of organosilane in silica-based hybrid materials has not yet been reported. This observation is in good agreement with the FTIR and elemental analysis, and strongly confirms the grafting of the hydrolyzed APTES on the diatomite surface.

In addition, a weak shoulder peak centered at 435 °C is resolved in the DTG curve of Dt-800/M, making the 540 °C peak asymmetric toward low temperatures. The shoulder peak should be assigned to the weakly bonded and oligomerized APTES species, just as in the case of Dt/M. This result reflects the existence of a small amount of non-grafted APTES species in Dt-800/M.

Dt-400/M and Dt-600/M exhibit thermal behaviors that are intermediate between the two extremes of Dt/M and Dt-800/M (Fig. 5b and c). In general, the main DTG peaks in the range of 400–550 °C of all mentioned samples are gradually shifted toward higher temperatures with the increase in the pretreatment temperature, indicating that grafting becomes increasingly more significant with the removal of water. As a simple indication of the quantity of introduced APTES species, the values of the mass loss (wt.%), in order, in the range of 150–1000 °C were as follows: Dt/M (14.4%) > Dt-800/M (7.8%) > Dt-400/M (4.5%) > Dt-600/M (3.3%), which matches the elemental analysis results well. However, quantitatively determining the content of APTES based on TG is not reasonable because the mass of the non-volatile silicon part of APTES, which remains even after the thermal decomposition of APTES, is difficult to evaluate.

3.3. Effects of the organosilane modification of diatomite on its Cu(II) adsorption performance

Grafting between diatomite and hydrolyzed APTES and oligomerization of APTES species are the two main mechanisms involved in the APTES modification of diatomite. Oligomerization

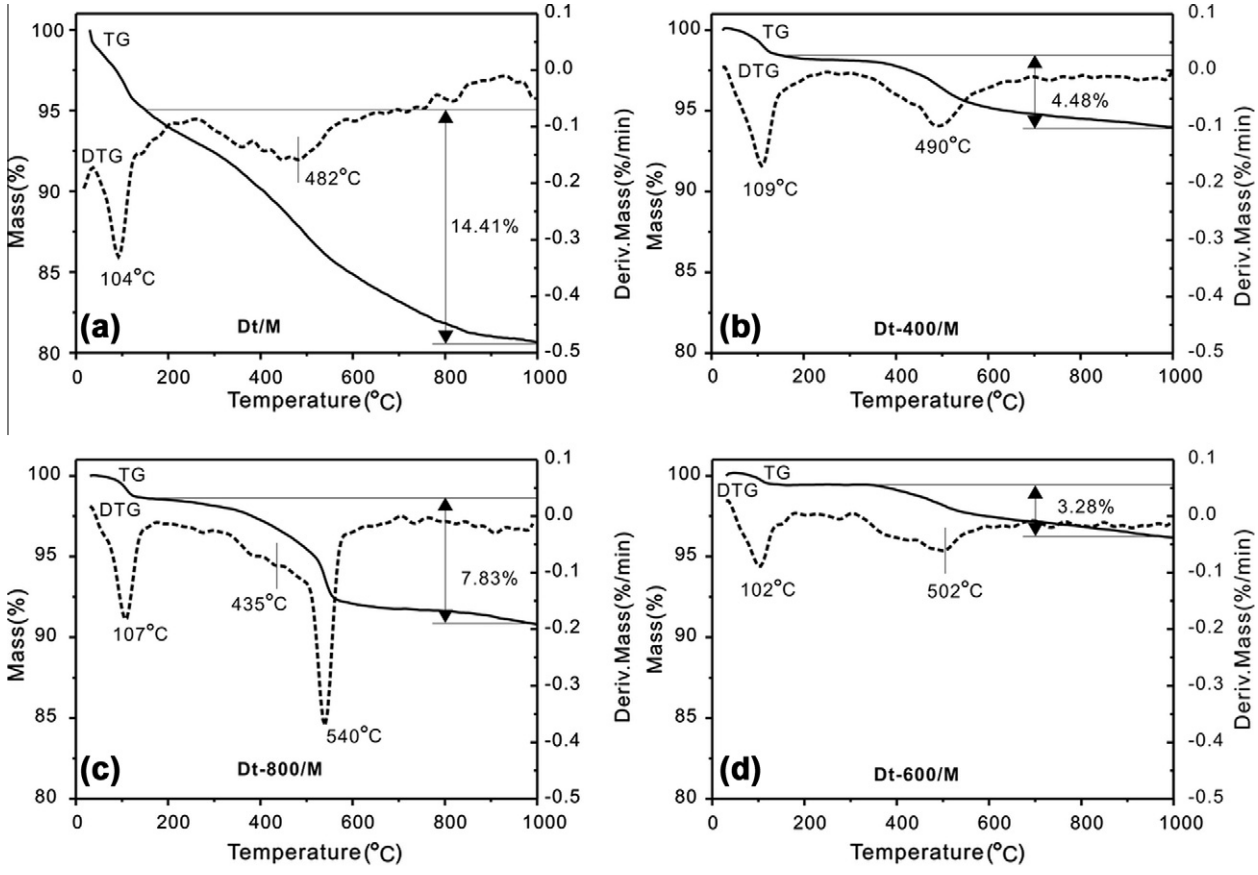

Fig. 5. TG and DTG curves of the APTES-modified diatomite samples.

occurs when there is a relatively large quantity of physically adsorbed water on the surface of diatomite, resulting in a high extent of APTES hydrolysis. The hydrolyzed APTES species then condense with each other or with the small quantity of directly grafted APTES to form a cross-linked structure, as schematically presented in Fig. 6a. More hydrolyzed APTES species are introduced into the cross-linked structure by weak interactions. Under a low heating temperature (e.g., in Dt/M), oligomerization is the dominant form of the hydrolyzed ATPES. Grafting of the hydrolyzed APTES on the surface of diatomite occurs when two conditions are satisfied: the physically adsorbed water molecules are mostly removed, such that the oligomerization is restrained, and the isolated silanols of diatomite are largely exposed, making them available for condensation with the hydrolyzed APTES. The appropriate temperature for achieving a grafting-dominant silylation is approximately 800 °C.

The different silylation mechanisms affect several properties of the modified diatomite products. First, many more APTES species are introduced into the oligomerization-dominant Dt/M than into the grafting-dominant Dt-800/M because of the formation of the multiple-layered and cross-linked network of hydrolyzed APTES in the oligomerization structure. In contrast with that, a much thinner APTES layer is formed in grafting-dominant diatomite (Fig. 6b). Second, the highly developed oligomerization sharply decreases the porosity of the oligomerization-dominant diatomite, whereas the thin layer of the grafted APTES decreases the porosity in a mild manner. Moreover, the oligomerization-dominant Dt/M exhibits less thermal stability than the grafting-dominant Dt-800/M because the grafted APTES is combined with the diatomite surface by strong chemical covalent bonds, whereas the oligomerized APTES is mainly attached through weak interactions. The APTES-modified samples derived from moderate heating, Dt-400/M and Dt-600/M, exhibit the above-described properties of being intermediate between the two extremes of the oligomerization-dominant and grafting-dominant products.

To further evaluate the effects of APTES modification on the adsorption properties of the silylated diatomite, Dt, Dt/M and Dt-800/M were used for the Cu(II) adsorption tests. Fig. 7a displays the removal of Cu(II) by Dt, Dt/M and Dt-800/M as a function of agitation time. The initial Cu(II) concentration was set at 100 mg/L. The Cu(II) adsorption on Dt was a fast process in which the equilibrium state was achieved in 30 min, but the total adsorption quantity was very low (Fig. 7a). In contrast, both Dt-800/M and Dt/M exhibited much higher Cu(II) uptakes. The initial Cu(II) uptake on the modified diatomite was quite fast and was followed by a slower subsequent removal and an eventual steady state after approximately 120 min (Fig. 7a). The rapid adsorption of Cu(II) by Dt-800/M and Dt/M is attributed to the external surface adsorption, suggesting that most of the adsorptive sites for Cu(II) existed in the exterior of the modified diatomite and were easily accessible to the Cu(II) species, resulting in a rapid approach to the steady state.

The kinetics curve of the adsorption process is simulated using the pseudo-second-order model [49,50], with the rate expression given by

$$dq_t/dt = k_p(q_e - q_t^2) \quad (1)$$

where k_p is the second order rate constant (g/mg.min) and q_t and q_e are the amounts of Cu(II) adsorbed per unit mass (mg/g) at any time (t) and at equilibrium, respectively. Eq. (1) can be rearranged to obtain the linear form:

$$t/q_t = 1/kq_e^2 + t/q_e \quad (2)$$

where $kq_e^2 = h$, and h is the initial adsorption rate (mg/(g · min)).

As shown in Table 2 and Fig. 7b, which provide the simulation results, the sorption of Cu(II) onto Dt, Dt/M and Dt-800/M fits Eq. (2) quite well. This result indicates that the kinetics of this sorption system are classified as pseudo-second-order, implying that the rate-limiting step may be chemical sorption involving valency forces through the sharing or exchanging of electrons between the amino groups and the Cu(II) species [51].

The initial sorption rates of Cu(II) species onto Dt-800/M and Dt/M are 26.3 and 1.6 mg/(g · min), respectively, which are significantly greater than the adsorption rates of Cu(II) species onto Dt. This result confirms the role of the amino groups that are post-introduced into Dt/M and Dt-800/M in the improvement of Cu(II) adsorption. Note that Dt-800/M has a much higher Cu(II) adsorption rate fthan Dt/M, although the actual amount of APTES in Dt-800/M is only approximately 78% of that in Dt/M. The reason for this result is that most amino groups in Dt/M are in the cross-linked network of oligomerized APTES, which are involved in several different interactions (Fig. 6) and therefore less available for Cu(II) adsorption than those in Dt-800/M case.

Fig. 7c displays the Cu(II) adsorption isotherms of Dt, Dt/M and Dt-800/M. The Langmuir adsorption isotherm model demonstrates the best fit in quantitatively describing the adsorption data compared with several commonly used fitting models, such as the Freundrich and Redlich-Peterson models [51]. The linear form of the Langmuir plot is given as

$$C_e/Q_e = 1/(bQ_m) + 1/(Q_m)C_e \quad (3)$$

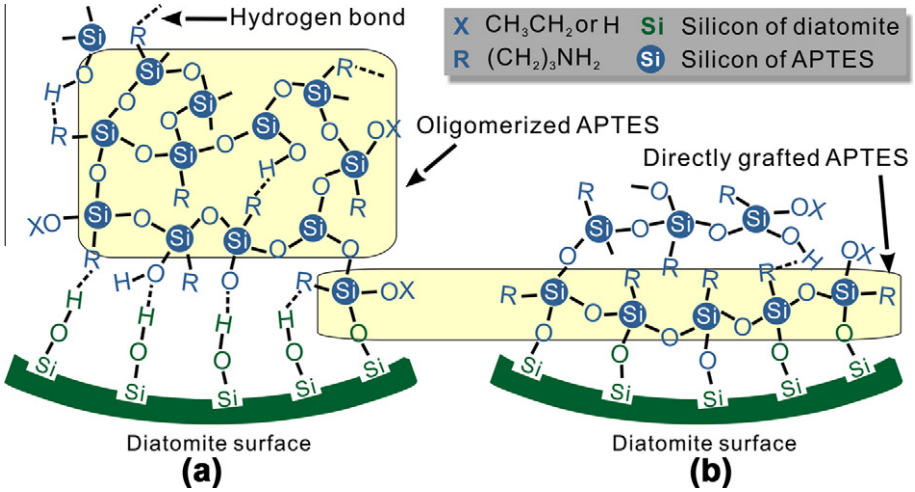

Fig. 6. Schematic presentation for the related mechanisms of the APTES modification: (a) oligomerization-dominant silylation; (b) grafting-dominant silylation.

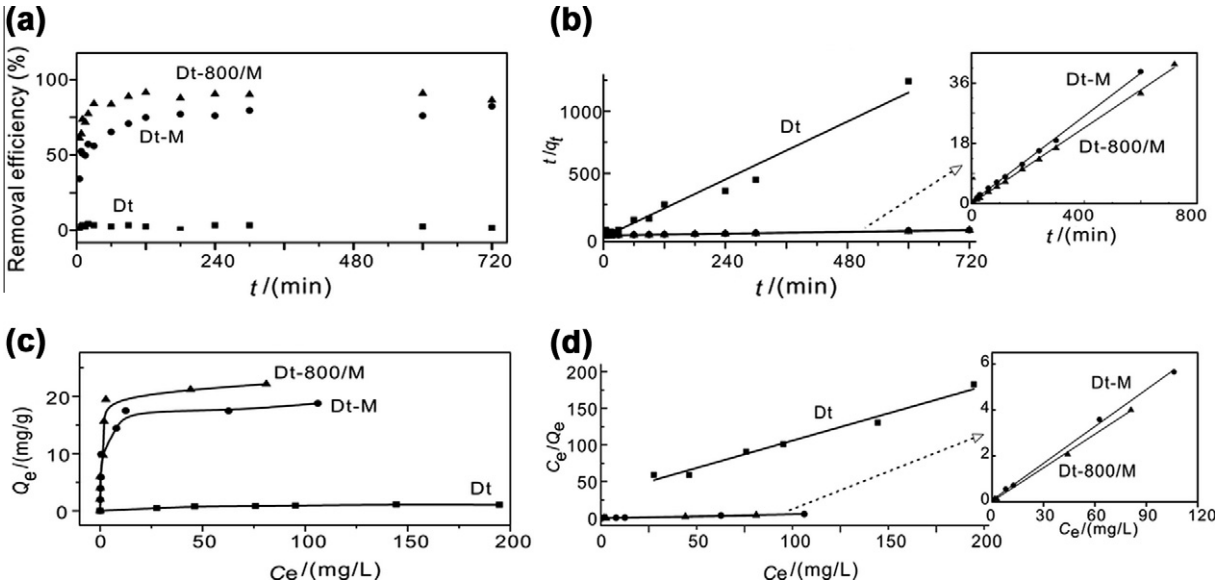

Fig. 7. (a) Effect of agitation time on the Cu(II) removal efficiency of Dt, Dt/M and Dt-800/M; (b) linear fitting plots based on pseudo-second-order kinetic model for the adsorption of Cu(II); (c) the Cu(II) adsorption isotherms of Dt, Dt/M and Dt-800/M; (d) linear fitting plots based on Langmuir isotherm model for the adsorption of Cu(II).

Table 2
Kinetics constants and Langmuir equation parameters for Cu(II) adsorption on various adsorbents.

Model parameters		Adsorbents		
		Dt	Dt/M	Dt-800/M
Kinetics constants	R^2	0.970	0.998	0.999
	K_p[g/(mg·min)]	−0.25	6.3×10^{-3}	8.2×10^{-3}
	q_e (mg/g)	0.5	16.1	17.9
	$t_{1/2}$ (min)	–	9.8	0.68
	h	−0.067	1.64	26.32
Langmuir equation parameters	R^2	0.976	0.996	0.998
	k_L	0.02	0.8	1.0
	Q_m (mg/g)	1.4	18.5	22.7
	R_L	0.8–0.2	$0.1–6.4 \times 10^{-3}$	$8.9 \times 10^{-2}–4.9 \times 10^{-3}$

where b and Q_m (mg/g) are the Langmuir constant and the monolayer adsorption capacity, respectively, and C_e (mg/L) is the equilibrium concentration of the Cu(II) in the liquid phase. As evidenced by the adsorption coefficients computed from Eq. (3) (Table 2 and Fig. 7d), the adsorption isotherms of Dt, Dt/M and Dt-800/M fit the Langmuir model well. The Q_m values of different adsorbents follow the order of Dt-800/M (22.7 mg/g) > Dt/M (18.5 mg/g) > Dt (1.4 mg/g). The Cu(II) adsorption capacity of Dt is slightly smaller than those of some amorphous silicas, such as synthetic silica gel (2.3 mg/g [52]) and the naturally occurring biogenic silica from rice husk (~5 mg/g [53]). The reason for this result is that the specific surface area of the diatomite used in the present study is much lower than those of the aforementioned silicas. The Cu(II) adsorption on the APTES-modified diatomite is more than 13-fold greater than that on the unmodified diatomites, demonstrating that the silylation of diatomite significantly increases its adsorption capacity. The Cu(II) adsorption capacity normalized to the actual APTES content (mmol/g), $Q_{m\text{-}s}$, was calculated based on the APTES content (Fig. 2c) and the Q_m values (Table 2) derived from the Langmuir equation. The $Q_{m\text{-}s}$ value of Dt-800/M (31.1 mg/mmol) is much larger than that of Dt/M (19.7 mg/mmol), confirming the higher adsorption efficiency of APTES in the form of grafting than that of oligomerization.

In the Langmuir adsorption isotherm model, R_L is often used to evaluate the affinity between the adsorbent and adsorbate. R_L is a dimensional constant called the separation factor, which is defined by the following equation [54]:

$$R_L = 1/(1 + a_L C_0) \quad (4)$$

where C_0 is the initial concentration (mg/L) of Cu(II) and a_L is the Langmuir constant, which is related to the adsorption energy (L/mg). Different affinities between the adsorbent and adsorbate are classified according to the value of R_L as follows: unfavorable adsorption ($R_L > 1$), linear adsorption ($R_L = 1$), favorable adsorption ($0 < R_L < 1$) or irreversible adsorption ($R_L \approx 0$) [55]. The R_L values of the diatomite samples are in the range of 0–1 (Table 2), indicating the favorable uptake of the Cu(II). In addition, the R_L values of both Dt/M and Dt-800/M are near zero, implying that the adsorption processes are almost irreversible. This result also supports that the Cu(II) uptake into the APTES-modified diatomite is a chemical adsorption process.

The XPS spectra of Cu obtained from the adsorbent surface after adsorption (initial Cu(II) concentration 100 mg/L; 480 min) are shown in Fig. 8. The Cu-adsorbed samples are indicated by the addition of "-Cu" suffix, e.g., Dt/M-Cu. The Cu2p XPS spectrum of Dt-Cu (Fig. 8a) does not exhibit any well resolved peaks, indicating the very low Cu content in the surface of the unmodified diatomite. The Cu2p XPS spectrum of Dt/M-Cu shows two peaks centered at 934.4 and 954.4 eV (Fig. 8b), attributed to the $Cu2p_{3/2}$ and $Cu2p_{1/2}$ levels of the $Cu^{0-\delta+}$ species, respectively. These peaks reflect the formation of the mono/bi/multidentate copper complexes with nitrogen ligands [56]. This result suggests that some chemical bonds were formed between copper ions and the amino groups, and the electron cloud density of the copper ions was therefore

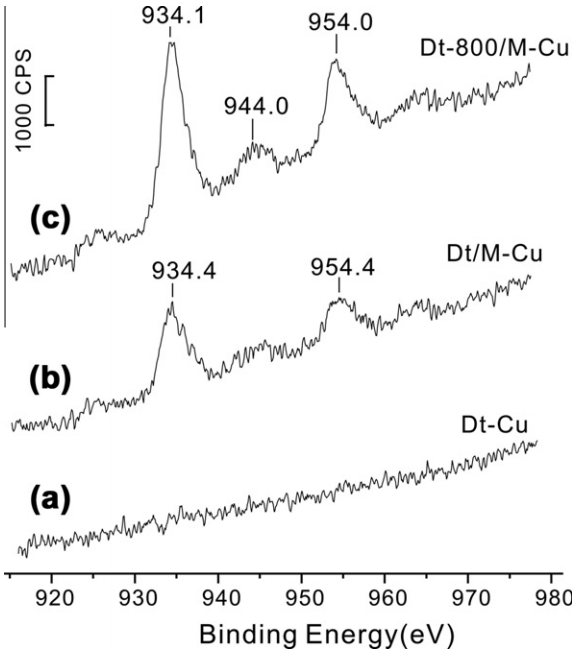

Fig. 8. The Cu2p XPS spectra of the different Cu-adsorbed samples: (a) Dt-Cu; (b) Dt/M-Cu; (c) Dt-800/M-Cu.

increased, resulting in the observed lower binding energy of the adsorbed copper ions than that of the $Cu2p_{3/2}$ and $Cu2p_{1/2}$ levels of Cu^{2+} (at approximately 935 and 955 eV, respectively [57]). Two similar but stronger peaks for $Cu2p_{3/2}$ and $Cu2p_{1/2}$ are resolved in the spectrum of Dt-800/M-Cu, reflecting a greater degree of Cu adsorption. The amino groups in Dt/M should be much more involved in the interactions (e.g., hydrogen bonding between nitrogen and hydrogen) in the cross-linked network of the oligomerized APTES, reducing their coordination with Cu and thus resulting in less Cu adsorption. Moreover, Dt-800/M-Cu shows slightly lower binding energy values for the peaks of $Cu2p_{3/2}$ and $Cu2p_{1/2}$ (at 934.1 and 954.0 eV, respectively) than that of Dt/M-Cu, implying a strong coordinative interaction for the copper species.

In addition, the minor satellite peaks centered at 944.0 eV exhibited in the XPS spectra of Dt/M-Cu and Dt-800/M-Cu are attributed to the adsorbed Cu^{2+} ions [56]. These Cu^{2+} ions may most likely be adsorbed through non-chemical bonding, e.g., by the electrostatic attraction between Cu^{2+} and the unmodified diatomite surface silanols.

The above results clearly demonstrate that the naturally occurring porous diatomite that underwent calcination at a temperature as high as 800 °C is capable of being used for organosilane modification and that the APTES-modified diatomite has a large adsorption capacity for copper ions. It is noteworthy that the heating temperature for a given diatomite should be optimized because the diatomite samples from diverse sources may have different properties. Based on these findings, the traditional applications of porous diatomite in the fields of filtering and adsorption can be significantly extended. Novel uses of adsorption, loading, or recovery for the organosilane-affinitive guests (such as metal ions and protein) can be accomplished by applying various organosilane species with diverse functional groups. Many further applications can also be postulated. For example, the organosilane modification of diatomite-based porous or foamy ceramics could enhance their performances for adsorption, separation and catalysis purposes; however, to date, no such attempt has been reported.

4. Conclusions

The porosity of the naturally occurring porous diatomite remains intact after calcination at temperatures as high as 800 °C. Heating significantly affects the surface silylation of diatomite by controlling the evolution of its hydration state. At a low heating temperature (150 °C), the hydrolyzed APTES is oligomerized and then attached to the diatomite surface by hydrogen bonding or Van der Waals interaction, resulting in a cross-linked structure containing a high content of APTES species. Heating at a high temperature (800 °C) leads to the removal of physically adsorbed water and the hydrogen-bonded capping water, exposing the surface isolated silanols of diatomite. These silanols act as the substrates for the grafting of the APTES molecules. In grafting-dominant structures, a relatively thin APTES layer is formed, and the grafted APTES exhibits a very high thermal stability. The decomposition temperature of grafted APTES is approximately 540 °C.

The Cu(II) adsorption on APTES-modified diatomite is 13 times greater than that on unmodified diatomite because of the high affinity of the amino groups for Cu ions. The grafting-dominant modified diatomite has a dramatically higher efficiency for Cu(II) adsorption than the oligomerization-dominant diatomite. The main reason for this greater efficiency is that the nitrogen atoms in the cross-linked network formed by oligomerized APTES are strongly affected by hydrogen bonding, which weakens their coordination with the copper species.

These fundamental results demonstrate that the calcined product of the naturally occurring porous diatomite is capable of being used for silylation. For the metal adsorption application of a given diatomite, the heating temperature must be carefully selected to generate a grafting-dominant silylation. Surface silylation accompanied by an appropriate heating pretreatment is very promising for the applications of diatomite in the fields of filtering, adsorption, and metal supporting for catalysis purposes.

Acknowledgments

Financial supports from Natural Science Foundation of China (Grant no. 40872042/41072032), and Natural Science Foundation of Guangdong Province, China, (Grant no. 8151064004000007) are gratefully acknowledged. This is a contribution (No. 1585) from GIGCAS.

Appendix A. Supplementary data

Supplementary data associated with this article can be found, in the online version, at http://dx.doi.org/10.1016/j.micromeso.2012.11.030.

References

[1] E. Stoermer, J. Smol, The diatoms: applications for the environmental and earth sciences, Cambridge University Press, Cambridge, 2001.
[2] D. Losic, J.G. Mitchell, N.H. Voelcker, Adv. Mater. 21 (2009) 2947.
[3] Y. Yu, J. Addai-Mensah, D. Losic, Langmuir 26 (2010) 14068.
[4] N. van Garderen, F.J. Clemens, J. Kaufmann, M. Urbanek, M. Binkowski, T. Graule, C.G. Aneziris, Micropor. Mesopor. Mater. 151 (2012) 255.
[5] P. Yuan, D. Liu, M.D. Fan, D. Yang, R.L. Zhu, F. Ge, J.X. Zhu, H.P. He, J. Hazard. Mater. 173 (2010) 614.
[6] J. Skubiszewska-Zięba, B. Charmas, R. Leboda, V. Gun'ko, Micropor. Mesopor. Mater. 156 (2012) 209.
[7] S.E. Ivanov, A.V. Belyakov, Glass Ceram. 65 (2008) 48.
[8] P.J. Lopez, J. Descles, A.E. Allen, C. Bowler, Curr. Opin. Biotech. 16 (2005) 180.
[9] N. Ediz, I. Bentli, I. Tatar, Int. J. Miner. Process 94 (2010) 129.
[10] G.D. Sheng, S.T. Yang, J. Sheng, J. Hu, X.L. Tan, X.K. Wang, Environ. Sci. Technol. 45 (2011) 7718.
[11] T.N.D. Dantas, A.A.D. Neto, M.C.P.D. Moura, Water Res. 35 (2001) 2219.
[12] G.D. Sheng, S.W. Wang, J. Hu, Y. Lu, J.X. Li, Y.H. Dong, X.K. Wang, Colloid Surf. A 339 (2009) 159.

[13] M.A.M. Khraisheh, Y.S. Al-Degs, W.A.M. Mcminn, Chem. Eng. J. 99 (2004) 177.
[14] G.D. Sheng, J. Hu, X.K. Wang, Appl. Radiat. Isot. 66 (2008) 1313.
[15] M. Aivalioti, I. Vamvasakis, E. Gidarakos, J. Hazard. Mater. 178 (2010) 136.
[16] J. Perić, M. Trgo, N. Vukojević Medvidović, Water Res. 38 (2004) 1893.
[17] S. Veli, B. Alyüz, J. Hazard. Mater. 149 (2007) 226.
[18] O. Abollino, M. Aceto, M. Malandrino, C. Sarzanini, E. Mentasti, Water Res. 37 (2003) 1619.
[19] B.J. Gao, P.F. Jiang, F.Q. An, S.Y. Zhao, Z. Ge, Appl. Surf. Sci. 250 (2005) 273.
[20] M. Al-Ghouti, M.A.M. Khraisheh, M.N.M. Ahmad, S. Allen, J. Colloid Interf. Sci. 287 (2005) 6.
[21] W.T. Tsai, C.W. Lai, K.J. Hsien, J. Colloid Interf. Sci. 297 (2006) 749.
[22] S. Ergul, S. Savasci, J. Chromatogr. Sci. 46 (2008) 308.
[23] S.R. Farrah, D.R. Preston, G.A. Toranzos, M. Girard, G.A. Erdos, V. Vasuhdivan, Appl. Environ. Microb. 57 (1991) 2502.
[24] H. Hadjar, B. Hamdi, M. Jaber, J. Brendie, Z. Kessaissia, H. Balard, J.B. Donnet, Micropor. Mesopor. Mater. 107 (2008) 219.
[25] M. Sprynskyy, I. Kovalchuk, B. Buszewski, J. Hazard. Mater. 181 (2010) 700.
[26] M. Šljivić, I. Smičiklas, S. Pejanović, I. Plećaš, Appl. Clay. Sci. 43 (2009) 33.
[27] X. Feng, G.E. Fryxell, L.Q. Wang, A.Y. Kim, J. Liu, K.M. Kemner, Science 276 (1997) 923.
[28] A.M. Liu, K. Hidajat, S. Kawi, D.Y. Zhao, Chem. Commun. (2000) 1145.
[29] B. Wang, T.R. Smith, J. Environ. Eng. Sci. 6 (2007) 469.
[30] Y. Yu, J. Addai-Mensah, D. Losic, J. Nanosci. Nanotechnol. 11 (2011) 10349.
[31] P. Yuan, D.Q. Wu, Z. Chen, Z.W. Chen, Z.Y. Lin, G.Y. Diao, J.L. Peng, Chin. Sci. Bull. 46 (2001) 1118.
[32] P. Yuan, D.Q. Wu, H.P. He, Z.Y. Lin, Appl. Surf. Sci. 227 (2004) 30.
[33] S.J. Gregg, K.S.W. Sing, Adsorption Surface Area and Porosity, Academic Press, London, 1982.
[34] J. Madejova, P. Komadel, Clay Miner. 49 (2001) 410.
[35] I.K. Tonle, E. Ngameni, D. Njopwouo, C. Carteret, A. Walcarius, Phys. Chem. Chem. Phys. 5 (2003) 4951.
[36] K.C. Vrancken, P. Vandervoort, I. Gillisdhamers, E.F. Vansant, P. Grobet, Chem. Soc. Faraday Trans. 88 (1992) 3197.
[37] L.C. Abbott, S.N. Batchelor, J. Oakes, B.C. Gilbert, A.C. Whitwood, J.R.L. Smith, J.N. Moore, J. Phys. Chem. A 109 (2005) 2894.
[38] L. Lucarelli, V. Nadtochenko, J. Kiwi, Langmuir 16 (2000) 1102.
[39] C.H.C. Liu, G.E. Maciel, J. Am. Chem. Soc. 118 (1996) 5103.
[40] B.A. Morrow, A.J. Mcfarlan, J. Phys. Chem. 96 (1992) 1395.
[41] L.T. Zhuravlev, Colloid Surf. A 74 (1993) 71.
[42] B. Humbert, J. Non-Cryst. Solids 191 (1995) 29.
[43] P. Yuan, H.P. He, D.Q. Wu, D.Q. Wang, L.J. Chen, Spectrochim. Acta A 60 (2004) 2941.
[44] E.P. Plueddemann, Silane Coupling Agents, Plenum Press, New York, 1991.
[45] G.S. Caravajal, D.E. Leyden, G.E. Maciel, in: D.E. Leyden (Ed.), Silanes, Surfaces and Interfaces, Gordon and Breach Science Publishers, New York, 1985.
[46] P. Yuan, P.D. Southon, Z.W. Liu, M.E.R. Green, J.M. Hook, S.J. Antill, C.J. Kepert, J. Phys. Chem C 112 (2008) 15742.
[47] J.-B. d'espinose de la Caillerie, M.R. Aimeur, Y.E. Kortobi, A.P. Legrand, J. Colloid Interf. Sci. 194 (1997) 434.
[48] A.S.M. Chong, X.S. Zhao, J. Phys. Chem. B 107 (2003) 12650.
[49] Y.S. Ho, G. McKay, Process. Biochem. 34 (1999) 451.
[50] Y.S. Ho, J.C.Y. Ng, G. Mckay, Sci. Technol. 36 (2001) 241.
[51] G. Limousin, J.P. Gaudet, L. Charlet, S. Szenknect, V. Barthes, M. Krimissa, Appl. Geochem. 22 (2007) 249.
[52] N. Chiron, R. Guilet, E. Deydier, Water Res. 37 (2003) 3079.
[53] X.G. Luo, Z.F. Deng, X.Y. Lin, C. Zhang, J. Hazard. Mater. 187 (2011) 182.
[54] K.R. Hall, L.C. Eagleton, A. Acrivos, T. Vermeule, Ind. Eng. Chem. Res. 5 (1966) 212.
[55] T.W. Weber, R.K. Chakravo, Aiche J. 20 (1974) 228.
[56] W. Cao, H.B. Zhang, Y.Z. Yuan, Catal. Lett. 91 (2003) 243.
[57] N.H. Turner, Appl. Spectrosc. Rev. 35 (2000) 203.